Automated Segmentation of Substantia Nigra and Red Nucleus in Quantitative Susceptibility Mapping Images

Dibash Basukala
Department of Computer Science and Software Engineering,
University of Canterbury
Christchurch, New Zealand
dibash.basukala@pg.canterbury.ac.nz

Ramakrishnan Mukundan
Department of Computer Science and Software Engineering,
University of Canterbury
Christchurch, New Zealand
mukundan@canterbury.ac.nz

Tracy Melzer
New Zealand Brain Research Institute,
Department of Medicine,
University of Otago
Christchurch, New Zealand
tracy.melzer@otago.ac.nz

Anthony Lim
Canterbury District Health Board,
Department of Radiology,
University of Otago
Christchurch, New Zealand
anthony.Lim@cdhb.health.nz

***Abstract*— Substantia nigra (SN) and red nucleus (RN) located in midbrain are integral in the study of brain disease such as Parkinson's disease (PD). The automatic segmentation of SN and RN in high-resolution quantitative susceptibility mapping (QSM) images can aid in PD characterization and progression. However, only a few methods have been proposed to segment them, owing to the recent development of high quality imaging. Therefore, we describe a novel method for the segmentation of SN and RN in QSM images using contrast enhancement, level set method, wavelet transform and watershed transform. The segmentation performance is evaluated in 20 subjects containing both healthy and PD patients. The results of the proposed segmentation method were closer to the manual segmentation performed by the radiologist than the popular level set methods. The Dice coefficient of the left SN and right SN were 0.77 ± 0.09 and 0.78 ± 0.07 respectively while the Dice for the left RN and right RN were 0.80 ± 0.08 and 0.77 ± 0.08 respectively.**

Keywords— Parkinson's disease, level set method, watershed transform, substantia nigra, red nucleus.

I. INTRODUCTION

Parkinson's disease (PD) is a neurodegenerative disease affecting the older population which primarily involves the degeneration of neurons in the substantia nigra (SN) [1]. Death of dopamine (DA) producing neurons in the SN affects smooth purposeful movement, poor balance and motor coordination [2], gradual slowness in spontaneous movement, rigidity and resting tremor. Almost 60 – 80 percent of the neuronal loss is observed at the time of symptom onset. Hence, early detection and monitoring neurodegenerative changes in PD can be helpful in clarifying the disease and its progression. Similarly, red nucleus (RN) located in the mid brain along with SN, is also involved in PD.

Conventional magnetic resonance imaging (MRI) at standard field strength are limited in their ability to show structural changes of SN and RN but high-resolution MRI at 3 Tesla (3T) is capable of providing detailed information about the structural changes of these iron-rich [3, 4] midbrain structures. Moreover, Quantitative susceptibility mapping (QSM), a phase based technique, produces high-resolution images with excellent contrast of these smaller brain nuclei. SN and RN are readily visible in T2-weighted images and T2*-weighted images but not clearly visible in T1-weighted images.

Segmentation of SN and RN can be helpful in PD characterization [5] and progression but is challenging because of their smaller structures, morphometric variability, unclear boundaries, and similar intensity profiles with the adjacent structures. Manual segmentation is tedious, time consuming and susceptible to inter and intra-rater bias. Therefore, automated segmentation is preferred to manual segmentation as it is capable of producing more consistent results. There are fairly limited number of literature available for the automated segmentation of SN and RN because high quality imaging capable of visualizing these midbrain structures is developed lately.

Xiao et al. [6] proposed a segmentation method by combining T1-weighted and T2*-weighted images into a single image for better non-rigid registration of atlas so that higher segmentation accuracy can be achieved. Haegelen et al. [7] compared the manual segmentation of deep brain structures with two registration based methods: automatic nonlinear image matching and anatomical labeling (ANIMAL) and symmetric image normalization (SyN) and also with one patch based method. ANIMAL and SyN are performed on T1-weighted images while SyN is performed on T2-weighted images. Xiao et al. [8] proposed the segmentation method using label - fusion by applying majority - voting approach. Moreover, principal component analysis (PCA) is used to measure the morphometric variability of the smaller brain nuclei. Kim et al. [9] used an active surface model and prior shape knowledge for the segmentation of brain subcortical structures. Similarly, Visser et al. [10] employed an intensity model and a shape model based on Markov random field (MRF) for the segmentation of the smaller brainstem nuclei. Also, Guo et al. [11] proposed a method combining atlas registration, seed points discontinuity and level set method for the segmentation of SN and RN.

Atlas based method is one of the most popular method used for the segmentation of SN and RN but the morphometric variability of these nuclei limits the accuracy

978-1-7281-2616-6/19/$31.00 ©2019 IEEE
DOI 10.1109/PDCAT.2019.00074

of segmentation in this method. Similarly, the limitation of the majority of the methods proposed in the literature is the requirement of the substantial number of expert supervised reference images to increase the labeling accuracy. As a result, computational cost is increased but the results are not still error-prone. Therefore, to address the drawback of the existing algorithms, we propose and evaluate a new and improved algorithm for the segmentation of SN and RN in QSM images by using contrast enhancement technique, level set method, dual-tree complex wavelet transform (DT-CWT) and watershed transform.

II. Materials and Methods

A total of 20 subjects containing both healthy and PD patients underwent MR scans on a 3T General Electric HDxt scanner (GE Healthcare, Waukesha, USA) with an eight-channel head coil. A 3D spoiled gradient recalled echo (SPGR) acquisition with 8 different echoes was used to obtain real and imaginary pairs with the following parameters: echo time (TE) = 3.5, 7.3, 11.1, 14.9, 18.7, 22.5, 26.3, 30.2 ms (3.8 ms intervals), repetition time (TR) = 42.8 ms, flip angle = 20°, acquisition matrix = 512×512×60, field of view (FOV) = 240 mm, slice thickness = 2 mm, voxel size = 0.47×0.47×2 mm^3. Spatial normalization was facilitated by acquiring a conventional T1-weighted 3D SPGR acquisition (TE/TR = 2.8/6.6 ms, inversion time (TI) = 400 ms, flip angle = 15°, acquisition matrix = 256×256×170, FOV = 250 mm, slice thickness = 1 mm, voxel size = 0.98×0.98×1.0 mm^3). In addition, T2-weighted and T2-weighted fluid-attenuated inversion recovery images were acquired to exclude any brain abnormalities.

Morphology enabled dipole inversion (MEDI) algorithm was used to generate QSM images from the real/imaginary pairs [12-14].

Segmentation Method

A. Contrast Enhancement

Contrast enhancement proposed in this work is based on local gray level and global gray level information of the image. Local gray level information is obtained by computing the mean of each non-overlapping 3×3 sub-images using mean filter while global gray level information is estimated by calculating the global mean of the entire image. The difference between the global gray level mean and the local gray level mean calculated over a neighbourhood of each pixels helps in identifying the gray level changes which depends on image characteristics in that neighbourhood [15, 16].

Let $A(x,y)$ be an input image. The global mean of this image can be calculated from entire image sample values as follows:

$$g_{mean}=\frac{1}{MN}\sum_{x=1}^{M}\sum_{y=1}^{N}A(x,y) \tag{1}$$

The local mean is calculated on each non-overlapping 3×3 sub-images using average filter. Let the sub-image of specified size be centered on (x,y). The contrast is enhanced on each sub-image as follows:

$$I(x+i,y+j)=A(x+i,y+j)+[l_{mean}(x+i,y+j)-g_{mean}] \tag{2}$$

where $i,j=-1,0,1$, $l_{mean}(x+i,y+j)$ is the local mean and $I(x+i,y+j)$ is the contrast enhancement performed on each sub-image. The overall contrast enhanced image $I(x,y)$ is obtained by repeating the process in (2) for all the sub-images.

B. Level Set Method

Chan and Vese (CV) [17] proposed a level set method based on Mumford-Shah model [18] for minimizing the energy given by,

$$\begin{aligned}&F^{CV}(C,c_1,c_2)\\&=\lambda_1\int_{\Omega_1}|I(x)-c_1|^2\,dx+\lambda_2\int_{\Omega_2}|I(x)-c_2|^2\,dx+\nu|C|\end{aligned} \tag{3}$$

where $\nu\geq0$, $\lambda_1,\lambda_2>0$, Ω_1 and Ω_2 is the regions outside contour C and inside contour C respectively, c_1 and c_2 approximate the image intensity in Ω_1 and Ω_2. But, CV model could not segment images with intensity inhomogeneities, common in medical images.

Hence, Li et al. [19, 20] addressed this issue by embedding the local image information which helps segmenting the images with intensity inhomogeneities. Thus, the energy functional is given by,

$$\begin{aligned}F(\phi,f_1,f_2)=&\sum_{i=1}^{2}\lambda_i\int\left(\int K_\sigma(x-y)|I(y)-f_i(x)|^2M_i^\varepsilon(\phi(y))dy\right)dx\\&+\nu\int|\nabla H_\varepsilon(\phi(x))|dx+\mu\int\frac{1}{2}(|\nabla\phi(x)|-1)^2dx\end{aligned} \tag{4}$$

where $f_1(x)$ and $f_2(x)$ approximate the local intensities in the regions outside and inside the contour respectively. K_σ is a Gaussian kernel with a scale parameter $\sigma>0$. H_ε is a smooth Heaviside function, $M_1^\varepsilon(\phi)=H_\varepsilon(\phi)$ and $M_2^\varepsilon(\phi)=1-H_\varepsilon(\phi)$, μ is a positive constant. Then, the minimization of energy functional $F(\phi,f_1,f_2)$ is performed with respect to ϕ by the gradient descent method,

$$\begin{aligned}\frac{\partial\phi}{\partial t}=&-\delta_\varepsilon(\phi)(\lambda_1e_1-\lambda_2e_2)+\nu\delta_\varepsilon(\phi)div\left(\frac{\nabla\phi}{|\nabla\phi|}\right)\\&+\mu\left(\nabla^2\phi-div\left(\frac{\nabla\phi}{|\nabla\phi|}\right)\right)\end{aligned} \tag{5}$$

where δ_ε is the smoothed Dirac delta function,

$$\begin{cases}e_1(x)=\int K_\sigma(y-x)|I(x)-f_1(y)|^2\,dy\\e_2(x)=\int K_\sigma(y-x)|I(x)-f_2(y)|^2\,dy\end{cases} \tag{6}$$

and,

$$\begin{cases} f_1(x)=\dfrac{K_\sigma * [H_\varepsilon(\phi) I]}{K_\sigma * H_\varepsilon(\phi)} \\ f_2(x)=\dfrac{K_\sigma * [(1-H_\varepsilon(\phi)) I]}{K_\sigma * (1-H_\varepsilon(\phi))} \end{cases} \quad (7)$$

In the proposed method, (5) is the level set equation to be solved. The first term in (5) is responsible for driving the active contour towards the boundaries of the object while the second term in (5) maintains the regularity of the contour. The third term in (5) is called a level set regularization term, plays a vital role in avoiding the time-consuming re-initialization since it maintains the regularity of the level set function significant for accurate computation and stable evolution in level set methods.

C. Wavelet Transform

Wavelet transform is a popular method for smoothing the images [21]. Wavelet based smoothing is performed by using a threshold to remove high frequency subband coefficients. Thresholding can be performed either by hard or soft thresholding method. In the proposed work, DT-CWT is used.

Dual-tree Complex Wavelet Transform

The ordinary discrete wavelet transform (DWT) is shift variant, leading to significant change of wavelet coefficients at the output even with a small shift in the input signal. It also provides limited directional selectivity (0° , 45° , 90°). Therefore, dual tree complex wavelet transform [22, 23] is introduced which exhibits approximate shift invariant property and improves directional resolution as it produces six directionally selective subbands ($\pm 15^\circ$, $\pm 45^\circ$, $\pm 75^\circ$) at each scale. DT-CWT is also robust to noise, limited redundant and performs perfect reconstruction.

The one-dimensional (1-D) DT-CWT [24] is shown in Fig. 1 which uses two DWTs. The first DWT gives the real part of the transform while the second DWT gives the imaginary part of the transform. A separate filter pair is used with $h_0(n)$ and $h_1(n)$ for the real part and $g_0(n)$ and $g_1(n)$ for the imaginary part otherwise no advantage is gained. The 1-D DT-CWT decomposes the input signal $f(x)$ in terms of

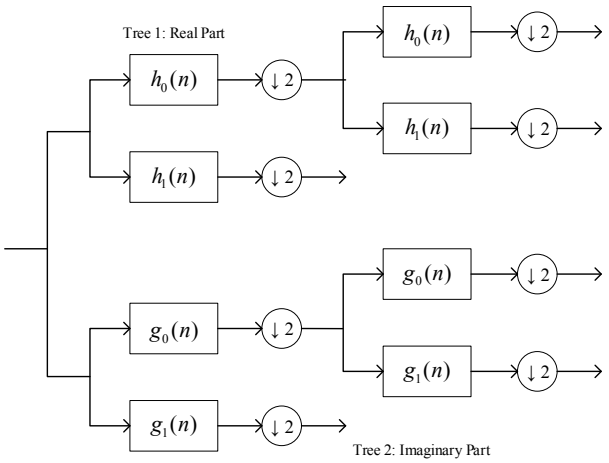

Fig. 1. 1-D dual-tree complex wavelet transform.

a complex shifted and dilated mother wavelet $\psi(x)$ and scaling function $\phi(x)$. Mathematically,

$$f(x)=\sum_{l\in N} B_{j_0,l}\phi_{j_0,l}(x)+\sum_{j\geq j_0}\sum_{l\in N} w_{j,l}\psi_{j,l}(x) \quad (8)$$

where N is the set of natural numbers, j_0 represents number of decomposition level, j and l are the index of shifts and dilations respectively. $B_{j_0,l}$ represents the scaling coefficient and $w_{j,l}$ represents the complex wavelet coefficient. Scaling function $\phi_{j_0,l}(x)=\phi^r_{j_0,l}(\mathrm{x})+i\phi^i_{j_0,l}(\mathrm{x})$ and complex wavelet function $\psi_{j,l}(x)=\psi^r_{j,l}(\mathrm{x})+i\psi^i_{j,l}(\mathrm{x})$ where the superscripts r and i represent the real and imaginary part respectively.

Similarly, the two-dimensional (2-D) DT-CWT decomposes an image $f(x,y)$ through a sequence of dilations and translations of a complex scaling function and six complex wavelet functions. Mathematically,

$$f(x,y)=\sum_{l\in N^2} B_{j_0,l}\phi_{j_0,l}(x,y)+\sum_{\theta\in\beta}\sum_{j\geq j_0}\sum_{l\in N^2} w^\theta_{j,l}\psi^\theta_{j,l}(x,y) \quad (9)$$

where $\theta\in\beta=\{\pm 15^\circ,\pm 45^\circ,\pm 75^\circ\}$ gives the directionality of the complex wavelet function. Therefore, the decomposition of a 2-D image $f(x,y)$ by DT-CWT gives a complex-valued low pass subband and six complex-valued high pass subbands at every level of decomposition where each high pass subband represents one unique direction θ.

D. Watershed Transformation

We first need to compute the distance transform before applying watershed transform. The distance transform labels each pixel of the image whose value correspond to the distance to the nearest feature pixel [25]. Watershed transform performed on the distance transformed image results in over-segmentation which is the biggest drawback of this algorithm because of the presence of several local minima. Hence, extended-minima transform is introduced to modify the distance transformed image for the accurate segmentation.

Extended-minima Transform

The extended minima transform *EMIN* are defined as the regional minima of the corresponding H -minima transformation [26, 27].

$$EMIN_h(f)=RMIN[HMIN_h(f)] \quad (10)$$

where,

$$HMIN_h(f)=R^\varepsilon_f(f+h) \quad (11)$$

is the H -minima transformation and is achieved by performing the reconstruction by erosion of f with respect to $f+h$. H -minima transform suppresses all minima whose depth is below or equal to the given h.

Implementation

The contrast enhanced image is obtained by using (2) for all the sub-images and it also is responsible for directing the evolution of level set function towards the desired direction.

The implementation of the proposed level set method is straightforward. The level set evolution in (5) can be implemented by obtaining the iteration scheme by discretizing the partial differential equation (PDE) as central finite differences. The level set function is initialized using a binary step function simply because it helps in the faster curve evolution and easier emergence of new contours than the initialization with a signed distance map. The binary step function takes negative constant value $-c_0$ inside the region and positive constant value c_0 outside the region. In our work, we use $c_0 = 2$.

Gaussian kernel K_σ with a scale parameter σ is used as a convolution kernel. The convolution kernel is constructed as a $w \times w$ mask, such that $w \geq 4 * \sigma + 1$. In our experiments, we use a scale parameter $\sigma = 10$, i.e., the size of mask is 41×41 . A smaller σ can be used but it will require large number of iterations for accurate computation.

In (7), there are altogether 4 convolutions in numerators and denominators. The two convolution $K_\sigma * I$ and $K_\sigma * 1$ required to compute f_2 does not depend on evolving level set function and therefore can be computed only once before the iterations. However, the other two convolutions $K_\sigma * [H_\varepsilon(\phi) I]$ and $K_\sigma * H_\varepsilon(\phi)$ required for computing the functions f_1 and f_2 needs to be computed at every iteration for evolving the level set function. Similarly, $(\lambda_1 e_1 - \lambda_2 e_2)$ in (5) is the combination of three convolutions. However, one of them is independent of evolving the level set function and can be computed only once before the iterations like in previous case. Therefore, there are four convolutions in total that needs to be computed at each iteration for evolving the level set function.

However, the level set method is not capable of producing the smooth output as desired. Moreover, over-segmentation is also observed in addition to its incapability of separating SN and RN. Therefore, DT-CWT is used while evolving the level set function to address these issues. DT-CWT consists of two wavelets in each direction and each wavelets are oriented in six distinct directions. So, in each direction, one of the two wavelets can be considered as the real part while the other wavelet can be considered as the imaginary part of the complex-valued wavelet. For the experiments in the paper, we take forward DT-CWT over 3 level of decomposition with different filter sets along the rows and columns. We obtain oriented wavelets by performing sum and difference of the subband images. Moreover, sum and difference operation is normalized by $1/\sqrt{2}$. Additionally, threshold is determined by heuristic approach for thresholding the high frequency wavelet coefficients through all scales and subbands. Finally, we take the inverse DT-CWT to get the smooth image contour and also to resolve the problem of over-segmentation.

But, the combination of level set method and DT-CWT is not capable of separating SN and RN accurately and efficiently. Therefore, distance transform is performed on the binary image resulting from the previous steps. Watershed transform applied on this distance transformed image cannot accurately separate SN and RN because of the presence of several local minima. Hence, extended-minima transform is used to suppress undesired local minima and then the distance transformed image is modified so that no minima appears at the filtered-out location. Watershed transform performed on this modified distance transformed image actually helps separating SN and RN effectively and efficiently.

Analysis of Segmentation

To assess the performance of the proposed segmentation method, subjective evaluation was done by a radiologist having years of experience in neuroimaging. Subjective evaluation was performed blindly, meaning the results of the proposed method and the various other methods used for comparison were mixed up for fair assessment. Subjective assessment was done using the score range from 1-5 for the obtained segmentation results.

The segmentation accuracy (quantitative analysis) is assessed using Dice score [28] which is a commonly used similarity metric to measure the spatial overlap between the two segmentations. The manual segmentation performed by the radiologist are compared with the results generated by our automated segmentation method. The value of Dice score ranges between 0 and 1; 0 means that there is no overlap between the two segmentation results while 1 means that the two segmentation results completely overlap with each other.

Manual Segmentations

The manual segmentations of the SN and RN was performed by the experienced radiologist for all the 20 subjects. The radiologist segmented the SN and RN on both left and right sides using the FSLeyes software for each subject. The manual segmentation was considered as the ground truth for performing the quantitative analysis.

Parameter Setup and Comparison with Different Methods

The proposed segmentation method for the accurate and effective segmentation of SN and RN requires various parameters to be specified. Therefore, we use the following parameters for the level set method in our experiments: $\lambda_1 = 1.0$, $\lambda_2 = 2.0$, $\mu = 1$, $v = 0.003 \times 255 \times 255$ and $\sigma = 10.0$.

We compare our proposed method with the level set methods to show the effectiveness of our proposed algorithm in all the 20 subjects because it is frequently used method for the segmentation of smaller structures in medical imaging. We used level set method based on the minimization of region scalable fitting (RSF) energy for segmentation of images with intensity inhomogeneities proposed by Li et al. [19] for comparison. Similarly, the level set method proposed by Li et al. [29] which is based on the local intensity clustering property and is capable of handling images with intensity inhomogeneities is also used for comparison.

III. RESULTS

The segmentation results of the proposed algorithm, comparison with different level set methods and manual segmentation of the SN and RN are shown in Fig. 2. The segmentation result of the left and right side of the SN and RN

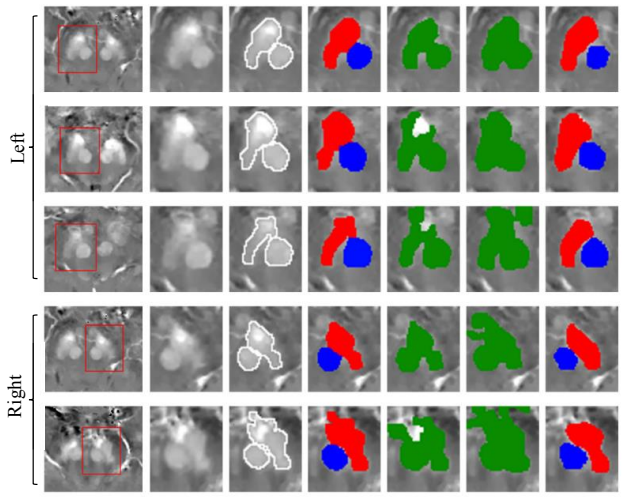

Fig. 2. Results of the proposed segmentation method and comparison with different methods. First four columns: Segmentation result of our proposed method. The result of automated segmentation is shown as a white contour and labeled mask is shown in red (SN) and blue (RN). Column 5: Result of the level set method based on minimization of region-scalable fitting energy. Column 6: Result of the level set method in the presence of intensity inhomogeneities with application to MRI. SN and RN both are labeled as green since level set method cannot separate them. Column 7: Manually labeled structures of SN (red) and RN (blue).

clearly shows that the proposed automated segmentation method produces good results and the labeled mask of SN and RN are closer to the manual segmentation. However, the RSF model and level set method based on the local intensity clustering property could not segment and separate SN and RN effectively.

Subjective evaluation is performed by an experienced radiologist for the analysis of different methods. Our proposed method obtained highest subjective score in comparison to the level set methods [19, 29] in the blind assessment and it validates our methodology. Besides, the Dice score for the proposed method is also calculated for the left and right side of the SN and RN for all the 20 subjects and is shown in Fig. 3. The Dice score (mean $\pm$ standard deviation) of the left SN and right SN between the manual segmentation and the proposed method were 0.77 ± 0.09 and 0.78 ± 0.07 respectively while the Dice for the left RN and right RN were 0.80 ± 0.08 and 0.77 ± 0.08 respectively.

IV. Discussion

We propose an effective method for the segmentation of SN and RN by combining contrast enhancement technique, level set method, DT-CWT and watershed transform. The contrast enhancement technique based on the local mean and global mean helps to improve the contrast of the region of interest thereby increasing the accuracy and effectiveness of segmentation. Moreover, the contrast enhanced image also plays an important role in directing the level set evolution towards the desired direction. The level set method proposed in this work make use of local image intensities rather than global intensities which makes it capable of handling images with intensity inhomogeneities. Additionally, the level set method also avoids the need of time consuming and expensive re-initialization process. However, the level set method results

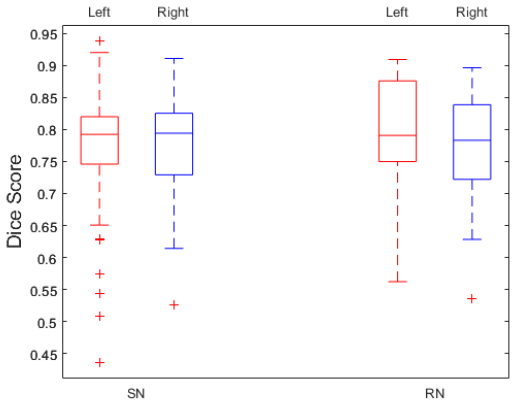

Fig. 3. Boxplot of Dice scores of the proposed segmentation method for the left and right sides of SN and RN.

in jagged output, over-segmentation and cannot separate SN and RN in some slices. Therefore, DT-CWT is used to produce the smooth result and also to solve the problem of over-segmentation. But, it cannot separate the smaller brain nuclei. Hence, watershed transform is introduced to separate and effectively segment SN and RN.

The level set [19, 29], an effective segmentation method which is based on the change of gray level is used for comparative analysis in our work. The level set method cannot segment and separate SN and RN effectively because of the similar intensity values between the adjacent areas and blurry boundary between the smaller nuclei. Moreover, it also constantly overestimates and underestimates them. Additionally, the level set method results in over-segmentation of the midbrain nuclei in the form of holes which do not make anatomical sense according to clinicians perspective.

The Dice score is used for the quantitative analysis in our work as it is the most commonly used metric to measure the fraction of spatial overlap between the binary regions for the evaluation of the segmentation result in the literature. The Dice score obtained in this study is in line with the current literature [10, 11] although comparison between them does not make much sense because of the difference in acquisition parameters and manual segmentation used. Moreover, the duration of disease in PD patients also makes considerable difference in the study.

In our work, the overall Dice score of SN could have been higher but the partial volume effect of SN particularly present on the left side limits the score which is evident by those many outliers on the lower side in the box plot in Fig. 3. The Dice score for the level set methods is not calculated as it is not able to separate the brain nuclei and calculating the score would not be fair.

V. Conclusion

We have presented an automated method for the segmentation of SN and RN in QSM images by combining contrast enhancement technique, level set method, DT-CWT and watershed transform. The experimental results shows that the proposed approach can produce high quality segmentation of SN and RN. The subjective evaluation of the results and the quantitative analysis performed based on the manual segmentation provided by the radiologist backs our claim. The

automated segmentation results were closer to manual segmentation than the popular level set methods. Our future work will be focused on developing more accurate, robust and efficient algorithm for the segmentation of SN and RN. We will also calculate the QSM values within the segmented region to find the deposition of iron and study its relationship to cognitive function, motor function and eventually in PD characterization and progression.

REFERENCES

[1] J. M. Fearnley, and A. J. Lees, "Ageing and Parkinson's disease: substantia nigra regional selectivity," *Brain,* vol. 114 (Pt 5), pp. 2283-301, Oct, 1991.

[2] W. R. B. Brain, and J. N. Walton, *Brain's Diseases of the nervous system*, 8th ed., Oxford Eng. ; New York: Oxford University Press, 1977.

[3] B. Hallgren, and P. Sourander, "The effect of age on the non-haemin iron in the human brain," *J Neurochem,* vol. 3, no. 1, pp. 41-51, Oct, 1958.

[4] E. Sofic, W. Paulus, K. Jellinger, P. Riederer, and M. B. Youdim, "Selective increase of iron in substantia nigra zona compacta of parkinsonian brains," *J Neurochem,* vol. 56, no. 3, pp. 978-82, Mar, 1991.

[5] R. A. Menke, S. Jbabdi, K. L. Miller, P. M. Matthews, and M. Zarei, "Connectivity-based segmentation of the substantia nigra in human and its implications in Parkinson's disease," *Neuroimage,* vol. 52, no. 4, pp. 1175-80, Oct 1, 2010.

[6] Y. Xiao, L. Bailey, M. M. Chakravarty, S. Beriault, A. F. Sadikot, G. B. Pike, and D. L. Collins, "Atlas-Based Segmentation of the Subthalamic Nucleus, Red Nucleus, and Substantia Nigra for Deep Brain Stimulation by Incorporating Multiple MRI Contrasts," *Information Processing in Computer-Assisted Interventions.* pp. 135-145, 2012.

[7] C. Haegelen, P. Coupe, V. Fonov, N. Guizard, P. Jannin, X. Morandi, and D. L. Collins, "Automated segmentation of basal ganglia and deep brain structures in MRI of Parkinson's disease," *Int J Comput Assist Radiol Surg,* vol. 8, no. 1, pp. 99-110, Jan, 2013.

[8] Y. Xiao, P. Jannin, T. D'Albis, N. Guizard, C. Haegelen, F. Lalys, M. Verin, and D. L. Collins, "Investigation of morphometric variability of subthalamic nucleus, red nucleus, and substantia nigra in advanced Parkinson's disease patients using automatic segmentation and PCA-based analysis," *Hum Brain Mapp,* vol. 35, no. 9, pp. 4330-44, Sep, 2014.

[9] J. Kim, C. Lenglet, Y. Duchin, G. Sapiro, and N. Harel, "Semiautomatic segmentation of brain subcortical structures from high-field MRI," *IEEE J Biomed Health Inform,* vol. 18, no. 5, pp. 1678-95, Sep, 2014.

[10] E. Visser, M. C. Keuken, B. U. Forstmann, and M. Jenkinson, "Automated segmentation of the substantia nigra, subthalamic nucleus and red nucleus in 7 T data at young and old age," *Neuroimage,* vol. 139, pp. 324-336, Oct 1, 2016.

[11] T. Guo, Y. Song, J. Li, M. Fan, X. Yan, A. He, D. Huang, C. Shen, G. Zhang, and G. Yang, "Seed point discontinuity-based segmentation method for the substantia nigra and the red nucleus in quantitative susceptibility maps," *J Magn Reson Imaging*, Mar 31, 2018.

[12] T. Liu, C. Wisnieff, M. Lou, W. W. Chen, P. Spincemaille, and Y. Wang, "Nonlinear formulation of the magnetic field to source relationship for robust quantitative susceptibility mapping," *Magnetic Resonance in Medicine,* vol. 69, no. 2, pp. 467-476, Feb, 2013.

[13] T. Liu, W. Y. Xu, P. Spincemaille, A. S. Avestimehr, and Y. Wang, "Accuracy of the Morphology Enabled Dipole Inversion (MEDI) Algorithm for Quantitative Susceptibility Mapping in MRI," *Ieee Transactions on Medical Imaging,* vol. 31, no. 3, pp. 816-824, Mar, 2012.

[14] Z. Liu, P. Spincemaille, Y. H. Yao, Y. Zhang, and Y. Wang, "MEDI+0: Morphology enabled dipole inversion with automatic uniform cerebrospinal fluid zero reference for quantitative susceptibility mapping," *Magnetic Resonance in Medicine,* vol. 79, no. 5, pp. 2795-2803, May, 2018.

[15] N. U. Khan, K. V. Arya, and M. Pattanaik, "Histogram statistics based variance controlled adaptive threshold in anisotropic diffusion for low contrast image enhancement," *Signal Processing,* vol. 93, no. 6, pp. 1684-1693, Jun, 2013.

[16] A. Singh, S. Yadav, and N. Singh, "Contrast Enhancement and Brightness Preservation using Global-Local Image Enhancement Techniques," *2016 Fourth International Conference on Parallel, Distributed and Grid Computing (Pdgc)*, pp. 291-294, 2016.

[17] T. F. Chan, and L. A. Vese, "Active contours without edges," *Ieee Transactions on Image Processing,* vol. 10, no. 2, pp. 266-277, Feb, 2001.

[18] D. Mumford, and J. Shah, "Optimal Approximations by Piecewise Smooth Functions and Associated Variational-Problems," *Communications on Pure and Applied Mathematics,* vol. 42, no. 5, pp. 577-685, Jul, 1989.

[19] C. Li, C. Y. Kao, J. C. Gore, and Z. Ding, "Minimization of region-scalable fitting energy for image segmentation," *IEEE Trans Image Process,* vol. 17, no. 10, pp. 1940-9, Oct, 2008.

[20] C. M. Li, C. Y. Kao, J. C. Gore, and Z. H. Ding, "Implicit active contours driven by local binary fitting energy," *2007 Ieee Conference on Computer Vision and Pattern Recognition, Vols 1-8*, pp. 339-+, 2007.

[21] S. G. Mallat, *A wavelet tour of signal processing*, 2nd ed., San Diego: Academic Press, 1999.

[22] N. Kingsbury, "The Dual-Tree Complex Wavelet Transform: A New Technique For Shift Invariance And Directional Filters," *8th IEEE DSP Workshop*, 1998.

[23] N. Kingsbury, "Complex Wavelets for Shift Invariant Analysis and Filtering of Signals," *Applied and Computational Harmonic Analysis,* vol. 10, no. 3, pp. 234-253, 2001/05/01/, 2001.

[24] T. Celik, and T. Tjahjadi, "Unsupervised colour image segmentation using dual-tree complex wavelet transform," *Computer Vision and Image Understanding,* vol. 114, no. 7, pp. 813-826, Jul, 2010.

[25] G. Borgefors, "Distance Transformations in Digital Images," *Computer Vision Graphics and Image Processing,* vol. 34, no. 3, pp. 344-371, Jun, 1986.

[26] J. R. Cheng, and J. C. Rajapakse, "Segmentation of Clustered Nuclei With Shape Markers and Marking Function," *Ieee Transactions on Biomedical Engineering,* vol. 56, no. 3, pp. 741-748, Mar, 2009.

[27] P. Soille, *Morphological Image Analysis: Principles and Applications*: Springer-Verlag, 2003.

[28] L. R. Dice, "Measures of the Amount of Ecologic Association between Species," *Ecology,* vol. 26, no. 3, pp. 297-302, 1945.

[29] C. Li, R. Huang, Z. Ding, J. C. Gatenby, D. N. Metaxas, and J. C. Gore, "A level set method for image segmentation in the presence of intensity inhomogeneities with application to MRI," *IEEE Trans Image Process,* vol. 20, no. 7, pp. 2007-16, Jul, 2011.